HIGHLIGHTS OF LHCb MEASUREMENT IN RARE DECAYS AND DISCOVERY OF FIRST PENTAQUARK STATES WITH RUN 1 DATA*

Artur Ukleja

on behalf of the LHCb experiment

National Centre for Nuclear Research, Warszawa, Poland

(Received April 6, 2016)

In pp collisions at the LHC, the LHCb experiment has collected the world's largest sample of beauty and charmed hadrons. Very precise measurements obtained from these data provide tests of the Standard Model, which are indirect searches for new physics. The highlights obtained using data of an integrated luminosity of 3.0 fb^{-1} recorded in 2011 and 2012 were shown, concerning the measurements of rare B and Λ_b decays. The first observation of two exotic structures in the $J/\psi p$ channel from $\Lambda_b^0 \to J/\psi pK^-$ decays was also presented. Masses of these states are $4380 \pm 8 \pm 29$ MeV and $4449.8 \pm 1.7 \pm 2.5$ MeV. The preferred J^P assignments are of opposite parity, one state having spin 3/2 and the other 5/2. These states are referred to as charmonium pentaquark states.

DOI:10.5506/APhysPolB.47.1581

1. Introduction

The Standard Model (SM) describes the fundamental particles interactions via the strong, electromagnetic and weak forces. It provides precise predictions for measurable quantities that can be tested experimentally. It is widely considered that the SM is not final since many phenomena in this model are not well-understood. This model is also not elegant since masses of a few fundamental particles, for instance electrons, are not predicted and they have to be taken from experiments. There are a few open questions in this model, for instance: why are there three generations of quarks and leptons? The measured value of CP violation is too small to explain the observed size of matter domination over antimatter in the universe.

* Presented at the Cracow Epiphany Conference on the Physics in LHC Run 2, Kraków, Poland, January 7–9, 2016.

Today, the main goal of particle physics is to search for physics beyond the SM. There are two ways of searches for new physics: direct and indirect. In the direct searches, the new particles are looked for. Such searches are performed in the ATLAS and CMS experiments, where the experimenters are looking for new objects produced directly in the pp interactions. In the LHCb experiment, the experimenters are testing the SM in precise measurements of known processes, what is widely referred to as indirect searches of the new physics. If the disagreement between the experiment and the SM prediction is found, it will be an indication for the existence of the new physics. The promising areas in these searches are the measurements of CP symmetry violation in B sector, spectroscopy of known or predicted particles and the very rare decays of B mesons. The rare decays are forbidden at the tree level in the SM. Therefore, they provide the interesting tests of this model, since the particles of new physics can be exchanged in loops of penguin and box diagrams, and they could significantly change the angular distributions of the final particles.

The structure of this report is as follows. The LHCb detector is first described in Sec. 2. The spectroscopy of exotic states: $Z(4430)^-$ and $J/\psi p$ resonances are presented in Sec. 3. Section 4 describes the very rare and rare decays of B, B_s and Λ_b. Finally, conclusions are presented in Sec. 5.

2. LHCb detector

The LHCb detector [1] is a single-arm forward spectrometer covering pseudorapidity range from 2 up to 5, designed for study of particles containing b or c quarks. Displaced vertices of b- and c-hadron decays can be measured with 20 μm resolution. The decay time resolution of 10% of the D-meson lifetime is achieved using a silicon vertex locator. The tracking system measures the charged particles with a momentum resolution $\Delta p/p$ that varies from 0.4% at 5 GeV to 0.6% at 100 GeV, corresponding to a typical mass resolution of approximately a few MeV for a two-body beauty meson decay. The $b\bar{b}$ cross section in 4π in pp collisions of 284 ± 53 μb is measured with the LHCb detector at $\sqrt{s} = 7$ TeV [2]. The measured $c\bar{c}$ cross section is about 20 times larger than the $b\bar{b}$ cross section [3].

3. Exotic spectroscopy at the LHCb

Heavy flavour spectroscopy is one of important tests of Quantum Chromodynamics (QCD). A large body of experimental evidence for QCD has been gathered over the years. Anyway, each measurement of masses, lifetimes, decay properties, quantum numbers *etc.* of known or predicted particles are one of the basic tests of the theory. One of these tests is related to the prospect of hadrons with more than the minimal quark content ($q\bar{q}$ or

qqq), which was proposed by Gell-Mann [4] and Zweig [5] in 1964. During evaluating of this idea, it was expanded upon to include baryons composed of four quarks plus one antiquark with name as pentaquark [6]. The first observation of tetraquark candidate, the $Z(4430)^-$ in $B^0 \to \psi' K\pi^-$ decays [7], suggests that the pentaquark baryon states can exist.

3.1. Observation of $Z(4430)^-$ resonance

The observation of $Z(4430)^-$ (the minimal quark content of such state is $c\bar{c}d\bar{u}$) could be interpreted as the first unambiguous evidence for the existence of mesons beyond the traditional $q\bar{q}$ model.

At the LHCb, the existence of $Z(4430)^-$ resonance is confirmed in an amplitude fit to the sample of $B^0 \to \psi' K^+\pi^-$ decays, where $\psi' \to \mu^+\mu^-$ [8]. Using the data corresponding to 3 fb^{-1} of integrated luminosity, 25176 ± 174 candidates of $B^0 \to \psi' K^+\pi^-$ decays are reconstructed. The distribution of invariant mass squared of $\psi'\pi^-$ is shown in Fig. 1. The significance of the Z^- is evaluated from the likelihood amplitude fits without and with the Z^- component. When the no-Z^- hypothesis is imposed to the fit, the measured probability of the consistency of the fit with data is very small (10^{-6}). The measured probability of the consistency of the fit with data is close to 12% if Z^- component is added to the fit. The mass and width of Z^- are measured to be $4475 \pm 7^{+15}_{-25}$ MeV and $172 \pm 13^{+37}_{-34}$ MeV, respectively. These values are consistent with the previous measurements in the Belle experiment [7].

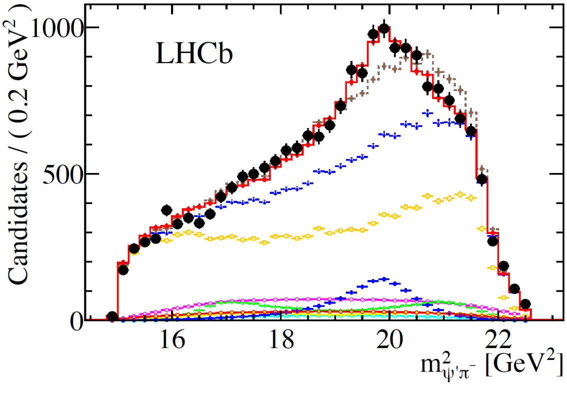

Fig. 1. (Colour on-line) The results of the fit illustrated in projections of $m^2_{\psi'\pi^-}$. The full (black) points represent the data, while the solid red (dashed brown) histogram corresponds to model with (without) the Z^- component. The other points illustrate various subcomponents of the fit that includes the Z^-: the upper (lower) blue points represent the Z^- component removed (taken alone). The orange, magenta, cyan, yellow, green and red points represent the $K^*(892)$, total S-wave, $K^*(1410)$, $K^*(1680)$, $K^*(1430)$ and background terms, respectively.

3.2. Observation of the $J/\psi p$ resonances consistent with pentaquark states in $\Lambda_b^0 \to J/\psi K^- p$ decays

The $\Lambda_b^0 \to J/\psi K^- p$ decays were first used at the LHCb to make precision measurements of the Λ_b^0 lifetime. In this analysis, we use data corresponding to 1 fb^{-1} of integrated luminosity at 7 TeV center-of-mass energy, and 2 fb^{-1} at 8 TeV. The 26007 ± 166 signal $\Lambda_b^0 \to J/\psi K^- p$ candidates are determined by the unbinned extended likelihood fit which is shown in Fig. 2 [9]. The background level is determined as 5.4% within ± 15 MeV ($\pm 2\sigma$) of the central value of the $J/\psi K^- p$ mass peak. In Fig. 3, the Dalitz plot is shown using the $K^- p$ and $J/\psi p$ invariant masses-squared as independent variables. A distinct vertical band is observed in the $K^- p$ invariant mass distribution

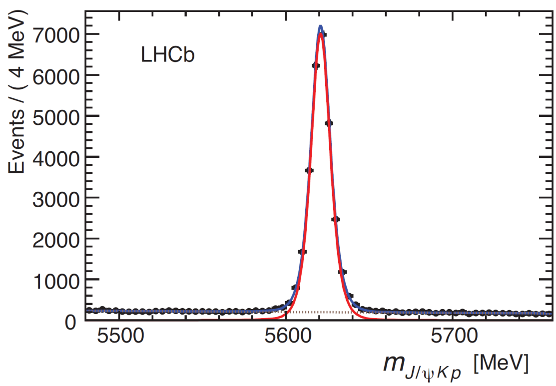

Fig. 2. (Colour on-line) Invariant mass spectrum of $J/\psi K^- p$ combinations with the total fit shown as solid (light grey/blue) line. Signal and background components also are shown as solid (dark grey/red) and dashed lines, respectively.

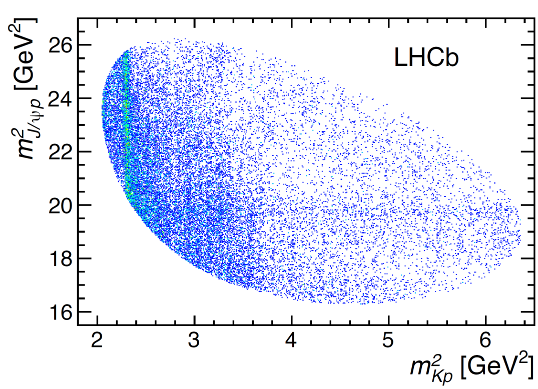

Fig. 3. Invariant mass squared of $K^- p$ *versus* $J/\psi p$ for candidates within ± 15 MeV of the Λ_b^0 mass.

near 2.3 GeV^2, corresponding to the $\Lambda(1520)$ resonance. There is also a distinct horizontal band observed in the $J/\psi p$ invariant mass distribution near 19.5 GeV^2. This behaviour is unexpected. No structure is seen in the $J/\psi K^-$ invariant mass.

As the final result of performed amplitude analysis, allowing for interference effects, it could be concluded that $\Lambda_b^0 \to J/\psi K^- p$ decays can proceed by the diagram shown in Fig. 4 (a). It is expected to be dominated by $\Lambda^* \to K^- p$ resonances. They are evident in the data shown in Fig. 5 (a). The diagram of the exotic contribution shown in Fig. 4 (b) is also possible and could result in resonant structures in the $J/\psi p$ mass spectrum shown in Fig. 5 (b).

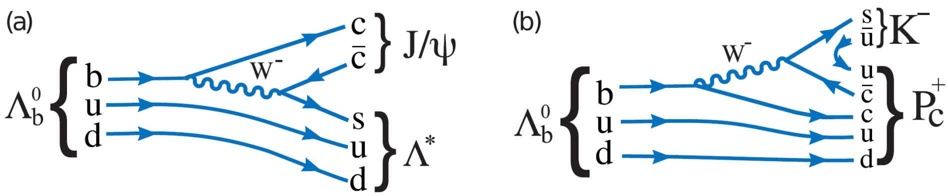

Fig. 4. Feynman diagrams for (a) $\Lambda_b^0 \to J/\psi \Lambda^*$ and (b) $\Lambda_b^0 \to P_c^+ K^-$ decays.

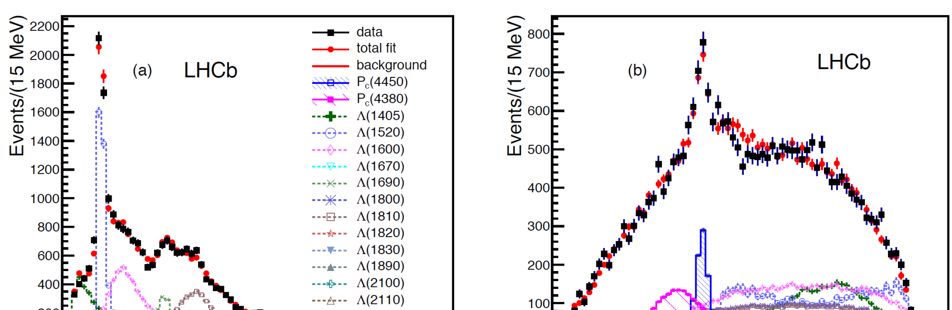

Fig. 5. (Colour on-line) Fit projections for (a) m_{Kp} and (b) $m_{J/\psi p}$ for the reduced Λ^* model with two P_c^+ states. The data points are shown as full (black) squares, while the full (red) points show the results of the fit. The solid (red) histogram shows the background distribution. The open (blue) squares with the shaded histogram represent the $P_c(4450)^+$ state, and the shaded histogram topped with filled (purple) squares represents the $P_c(4380)^+$ state. Each Λ^* component is also shown. The error bars on the points showing the fit results are due to simulation statistics.

The structures seen in Fig. 5 (b) are not due to reflections generated by the Λ^* states. To prove that, it was first tried to fit the data with an amplitude model that contains 14 known Λ^* states listed by the Particle Data Group [10]. This did not give a satisfactory description of the data. Taking into account one P_c^+ state in the fitted amplitude model is not sufficient to describe the data. The two P_c^+ states are needed to describe the data. The result of the best fit projections is shown in Fig. 5. Both m_{Kp} and the peaking structure in $m_{J/\psi p}$ are reproduced by the fit. These two P_c^+ states are found to have masses of $4380 \pm 8 \pm 29$ MeV and $4449.8 \pm 1.7 \pm 2.5$ MeV, with corresponding widths of $205 \pm 18 \pm 86$ MeV and $39 \pm 5 \pm 19$ MeV. The fractions of the total sample due to the lower mass and higher mass states are $8.4 \pm 0.7 \pm 4.2\%$ and $4.1 \pm 0.5 \pm 1.1\%$, respectively. The best fit solution has spin-parity J^P values of $(3/2^-,\ 5/2^+)$. Acceptable solutions are also found for additional cases with opposite parity, either $(3/2^+,\ 5/2^-)$ or $(5/2^+,\ 3/2^-)$. The significances of the lower mass and the higher mass states are 9 and 12 standard deviations, respectively.

Further evidence for the resonant character of the higher mass state is obtained by viewing the evolution of the complex amplitude in the Argand diagram (Fig. 6 (a)). The $P_c(4450)^+$ is represented by a Breit–Wigner amplitude, where the magnitude and phase vary with $m_{J/\psi p}$ according to an

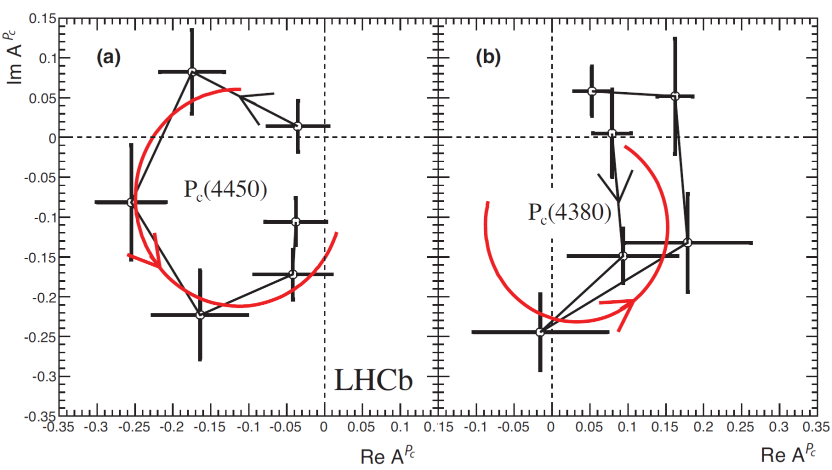

Fig. 6. (Colour on-line) Fitted values of the real and imaginary parts of the amplitudes for (a) the $P_c(4450)^+$ state and (b) the $P_c(4380)^+$ state, each divided into six $m_{J/\psi p}$ bins of equal width between $-\Gamma_0$ and $+\Gamma_0$ shown in the Argand diagrams as connected points with error bars. The solid (red) curves are the predictions from the Breit–Wigner formula for the same mass ranges with M_0 (Γ_0) of 4450 (39) MeV and 4380 (205) MeV, respectively, with the phases and magnitudes at the resonance masses set to the average values between the two points around M_0.

approximately circular trajectory in the real and imaginary plane of the $m_{J/\psi p}$-dependent part of the $P_c(4450)^+$ amplitude. The resulting Argand diagram, shown in Fig. 6 (a), is consistent with a rapid counter-clockwise change of the $P_c(4450)^+$ phase when its magnitude reaches the maximum. It is a behaviour characteristics of a resonance. A similar study for the lower mass state is shown in Fig. 6 (b). For the lower mass state, the evolution of the complex amplitude in the Argand diagram is not conclusive, since the fit does not show a large phase change.

4. Very rare and rare decays of B, B_s and Λ_b at the LHCb

The presented in this section very rare and rare B, B_s and Λ_b decays are forbidden at tree level in the SM. At the lowest order, they can only occur via electroweak penguin and box processes. In extensions of the SM, new, heavy particles can enter in competing processes and can significantly change the branching fraction of the decay and the angular distribution of the final state particles.

4.1. Very rare $B^0 \to \mu^+\mu^-$ and $B_s^0 \to \mu^+\mu^-$ decays

The branching fractions of the B^0 and B_s^0 mesons decaying into two oppositely charged muons are interesting since their sensitivity to theories that extend the SM. A difference in the observed branching fractions with respect to the predictions of the SM would provide a direction in which the theory should be extended. It predicts that the $B^0 \to \mu^+\mu^-$ and the $B_s^0 \to \mu^+\mu^-$ decays are very rare, $(1.066 \pm 0.09) \times 10^{-10}$ and $(3.66 \pm 0.23) \times 10^{-9}$ of branching fractions, respectively [11].

The CMS and LHCb experiments have performed a joint analysis of the data collected in 2011 and 2012 [12]. The combined results are shown in Fig. 7. The fit to the combined data leads to the measurements of branching fractions as $(3.9^{+1.6}_{-1.4}) \times 10^{-10}$ for $B^0 \to \mu^+\mu^-$ and $(2.8^{+0.7}_{-0.6}) \times 10^{-9}$ for $B_s^0 \to \mu^+\mu^-$, where the uncertainties include both statistical and systematic sources, the latter contributing 18% and 35% of the total uncertainty for the B^0 and B_s^0 decays, respectively. It is the first observation of the $B_s^0 \to \mu^+\mu^-$ decay with a statistical significance exceeding six standard deviations (6.2σ). Also the best evidence for the $B^0 \to \mu^+\mu^-$ decay is measured with a statistical significance of three standard deviations (3.2σ). The measured branching fractions of both decays are statistically compatible with the SM predictions and allow stringent constraints to be placed on theories beyond the SM.

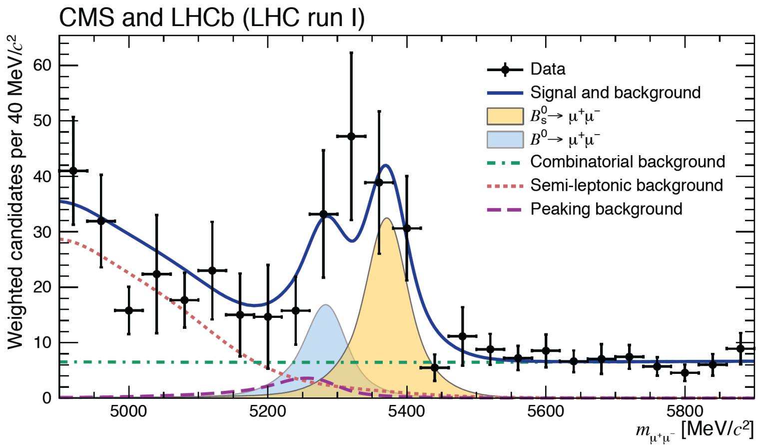

Fig. 7. (Colour on-line) Distribution of the dimuon invariant mass, $m_{\mu^+\mu^-}$, as a combined result obtained in CMS and LHCb experiments. Superimposed on the data points in black are the combined fit (solid blue line) and its components: the B_s^0 (grey/yellow shaded area) and B^0 (light grey/light blue shaded area) signal components; the combinatorial background (dash-dotted green line); the sum of the semi-leptonic backgrounds (dotted salmon line); and the peaking background (dashed violet line).

4.2. Rare $B^0 \to K^{*0}\mu^+\mu^-$ decays

An angular analysis of the $B^0 \to K^{*0}\mu^+\mu^-$ decays was performed using the LHCb dataset corresponding to an integrated luminosity of 3 fb^{-1}. The K^{*0} is reconstructed through the $K^{*0} \to K^+\pi^-$ decay. Angular observables are of particular interest, since theoretical predictions of such observables tend to be less affected by form-factor uncertainties in the $B^0 \to K^{*0}$ transition. Using the full angular distribution, a complete set of CP-averaged observables are extracted for the first time [13]. The $B^0 \to K^{*0}\mu^+\mu^-$ signal yield integrated over q^2 is determined to be 2398 ± 57 candidates (Fig. 8).

The final state of the $B^0 \to K^{*0}\mu^+\mu^-$ decay can be fully described by four variables: the q^2, the invariant mass of the dimuon system squared, and three decay angles, which describe particles reconstructed in the final state. More details on the angular formalism adopted in this analysis, as well as the differential decay rate, in terms of q^2 and three angles, are given in Ref. [13]. The likelihood fits to the reconstructed mass and three angles distributions for the different q^2 bins are performed to determine the CP-averaged observables. In general, the correlations between the observables are small. The exception to this is the correlation of $A_{\rm FB}$ and $F_{\rm L}$, which can be as large as $\sim 50\%$. Neglecting the correlations between the CP observables, the results appear largely in agreement with the SM predictions, with the exception of

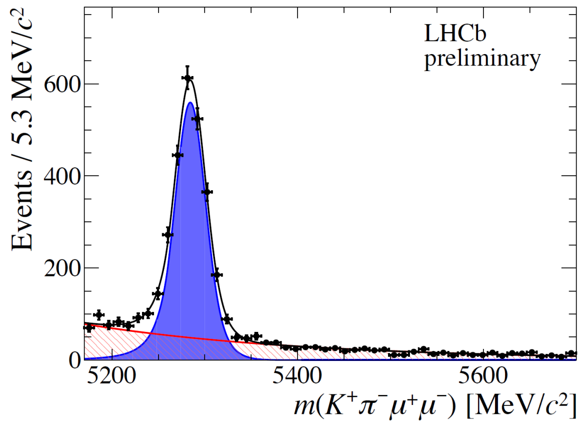

Fig. 8. (Colour on-line) Invariant mass $m(K^+\pi^- u^+\mu^-)$ distribution integrated over the full q^2 range. The signal is shown by the dark grey/blue component and the background is shown by the hatched (red) component.

the one, P_5' (Fig. 9). The P_5' is defined as $P_5' = S_5/\sqrt{F_{\rm L}(1-F_{\rm L})}$, where S_5 is additional CP observable, which is measured and $F_{\rm L}$ is the longitudinal polarization fraction of the K^{*0}. The P_5' is "optimised" since the leading form-factor uncertainties cancel in its calculation.

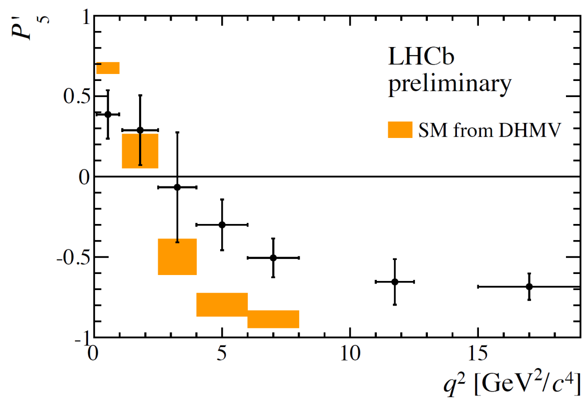

Fig. 9. The observable P_5' in q^2 bins. The shaded boxes show the Standard Model predictions [14].

The observed tension with the SM prediction [14] in P_5' is at a level of 2.9σ in each of the $4.0 < q^2 < 6.0$ GeV^2 and $6.0 < q^2 < 8.0$ GeV^2 bins. A naïve combination of these deviations, based on a χ^2 probability with two degrees of freedom and assuming the SM predictions in the two bins are uncorrelated, yields a local tension of 3.7σ.

A mild tension can also be seen in the measured $A_{\rm FB}$ distribution (Fig. 10). The $A_{\rm FB}$ is the forward–backward asymmetry of the dimuon system. The $A_{\rm FB}$ fit results are systematically less than 1σ below the SM prediction [15] in the region with $1.1 < q^2 < 6.0$ GeV^2. The zero-crossing point of $A_{\rm FB}$, q_0^2, has been determined to be $(3.7^{+0.8}_{-1.1})$ GeV^2. This value of q_0^2 is in a good agreement with the SM prediction which is around 4.0 GeV^2 [16].

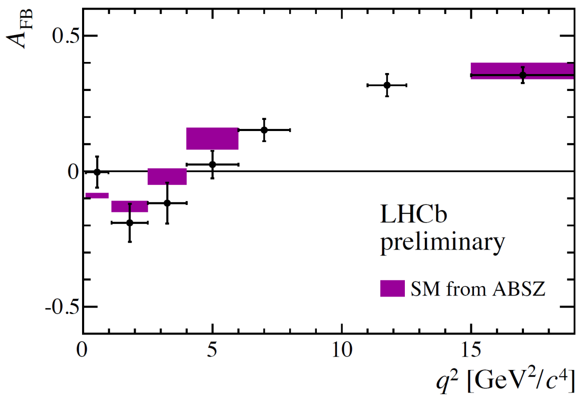

Fig. 10. The CP-averaged observable $A_{\rm FB}$ in q^2 bins. The shaded boxes show the Standard Model predictions [15].

4.3. Differential branching fraction in $B^{0,+}$ and Λ_b decays

The partial branching fractions of the $B^0 \to K^0\mu^+\mu^-$, the $B^+ \to K^{*+}\mu^+\mu^-$, the $B^+ \to K^+\mu^+\mu^-$ and the $B_s^0 \to \phi\mu^+\mu^-$ decays are measured as functions of the q^2 and the results are shown in Fig. 11, with theoretical predictions [16] superimposed. The data used in the analysis correspond to 3 fb^{-1}. Signal yields are determined using extended unbinned maximum likelihood fits to the invariant mass distributions as the 176 ± 17 $B^0 \to K^0\mu^+\mu^-$, the 162 ± 16 $B^+ \to K^{*+}\mu^+\mu^-$, the 4746 ± 81 $B^+ \to K^+\mu^+\mu^-$ and the 432 ± 24 $B_s^0 \to \phi\mu^+\mu^-$ candidates [17, 18]. The differential branching fraction measurements are consistent with the SM, but they have values systematically smaller than the theoretical prediction. In particular, for $B_s^0 \to \phi\mu^+\mu^-$, in the q^2 region $1.0 < q^2 < 6.0$ GeV^2, the measured branching fraction of $(2.58 \pm 0.08 \pm 0.19) \times 10^{-8}$ GeV^{-2} lies 3.3σ below the SM expectation of $(4.91 \pm 0.56) \times 10^{-8}$ GeV^{-2}.

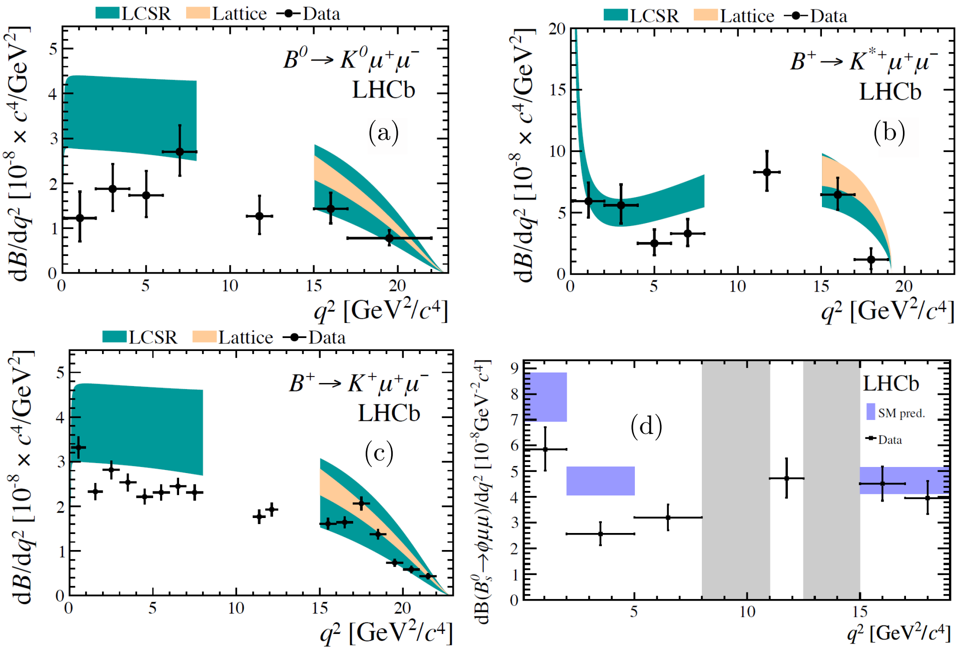

Fig. 11. Differential branching fraction results for (a) the $B^0 \to K^0\mu^+\mu^-$, (b) the $B^+ \to K^{*+}\mu^+\mu^-$, (c) the $B^+ \to K^+\mu^+\mu^-$ and (d) the $B_s^0 \to \phi\mu^+\mu^-$ decays. The shaded regions illustrate the theoretical predictions and their uncertainties from light cone sum rule and lattice QCD calculations [16].

Summing the q^2 bins and applying the extrapolation to the full q^2 range, the integrated branching fractions become

$$\begin{aligned}
\mathcal{B}\left(B^0 \to K^0\mu^+\mu^-\right) &= (3.27 \pm 0.34 \pm 0.17) \times 10^{-7}\,,\\
\mathcal{B}\left(B^+ \to K^{*+}\mu^+\mu^-\right) &= (9.24 \pm 0.93 \pm 0.67) \times 10^{-7}\,,\\
\mathcal{B}\left(B^+ \to K^+\mu^+\mu^-\right) &= (4.29 \pm 0.07 \pm 0.21) \times 10^{-7}\,,\\
\mathcal{B}\left(B_s^0 \to \phi\mu^+\mu^-\right) &= (7.97 \pm 0.22 \pm 0.23) \times 10^{-7}\,,
\end{aligned}$$

where the uncertainties are statistical and systematic.

Closely related to the above decays are the $\Lambda_b^0 \to \Lambda\mu^+\mu^-$ decays, for which the differential branching fraction is also measured as a function of q^2 (Fig. 12). The 9.4 ± 6.3 in the interval $1.1 < q^2 < 6.0$ GeV^2 and 276 ± 20 in the interval $15.0 < q^2 < 20.0$ GeV^2 candidates of such decays are reconstructed in 2011 and 2012 data samples, respectively [19]. The data are consistent with the theoretical predictions in the high-q^2 region but lie below the predictions in the low-q^2 region.

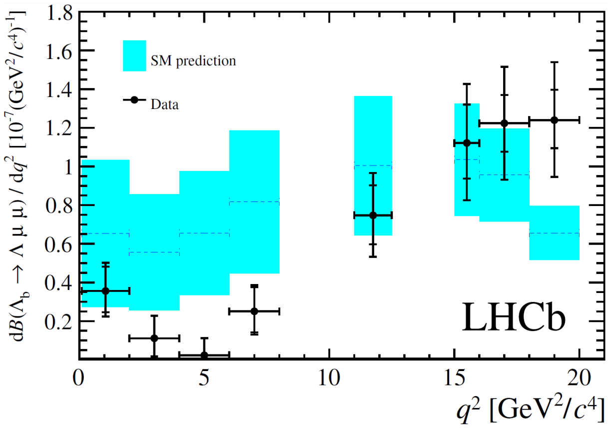

Fig. 12. Measured $\Lambda_b^0 \to \Lambda\mu^+\mu^-$ branching fraction as a function of q^2 with the predictions of the SM superimposed. The inner bars on data points represent the total uncertainty on the relative branching fraction (statistical and systematic). The outer error bar also includes the uncertainties from the branching fraction of the normalisation mode.

5. Summary

The data, corresponding to an integrated luminosity of 3 fb^{-1}, recorded using the LHCb detector, are used to precisely test the SM predictions. For the first time, the two exotic structures in the $J/\psi p$ system are observed, which are referred to as charmonium pentaquark states. Masses of these states are found to be $4380 \pm 8 \pm 29$ MeV and $4449.8 \pm 1.7 \pm 2.5$ MeV. The spin-parity J^P values are found to be $(3/2^-, 5/2^+)$. Acceptable solutions are also found for additional cases with opposite parity, either $(3/2^+, 5/2^-)$ or $(5/2^+, 3/2^-)$. The resulting Argand diagram for the higher mass state $P_c(4450)^+$ is characteristic for a resonance behaviour. For the lower mass state $P_c(4380)^+$, the evolution of the complex amplitude in the Argand diagram is not conclusive.

For the first time, the $B_s^0 \to \mu^+\mu^-$ decay is observed with a statistical significance exceeding six standard deviations in combination of results of the CMS and LHCb experiments. The best evidence for the $B^0 \to \mu^+\mu^-$ decay is also measured with a statistical significance of three standard deviations. Both measurements are statistically compatible with the SM predictions and allow stringent constraints to be placed on theories beyond the SM.

Although the measurements performed in the LHCb experiment confirm the robustness of the SM, several hints of effects beyond the SM are seen at the level of 3σ. One CP observable P_5', measured in the rare $B^+ \to K^{*+}\mu^+\mu^-$ decays, lies above the SM predictions, in the dimuon mass squared, q^2: $4.0 < q^2 < 8.0$ GeV^2 region, yielding a tension at the level of 3.7σ. The measured differential branching fractions of the $B^0 \to K^0\mu^+\mu^-$, the $B^+ \to K^{*+}\mu^+\mu^-$, the $B^+ \to K^+\mu^+\mu^-$, the $B_s^0 \to \phi\mu^+\mu^-$ and the $\Lambda_b^0 \to \Lambda\mu^+\mu^-$ decays also have systematically lower values than the SM predictions. In particular, for the $B_s^0 \to \phi\mu^+\mu^-$ decays in the $1.0 < q^2 < 6.0$ GeV^2 region, the differential branching fraction is more than 3σ below the SM prediction.

REFERENCES

[1] A. Alves *et al.* [LHCb Collaboration], *JINST* **3**, S08005 (2008).

[2] R. Aaij *et al.* [LHCb Collaboration], *Phys. Lett. B* **694**, 209 (2010).

[3] R. Aaij *et al.* [LHCb Collaboration], *Nucl. Phys. B* **871**, 1 (2013).

[4] M. Gell-Mann, *Phys. Lett.* **8**, 214 (1964).

[5] G. Zweig, An SU_3 Model for Strong Interaction Symmetry and Its Breaking, CERN-TH-401, 1964.

[6] H.J. Lipkin, *Phys. Lett. B* **195**, 484 (1987).

[7] S.K. Choi *et al.* [Belle Collaboration], *Phys. Rev. Lett.* **100**, 142001 (2008).

[8] R. Aaij *et al.* [LHCb Collaboration], *Phys. Rev. Lett.* **112**, 222002 (2014).

[9] R. Aaij *et al.* [LHCb Collaboration], *Phys. Rev. Lett.* **115**, 072001 (2015).

[10] K.A. Olive *et al.* [Particle Data Group], *Chin. Phys. C* **38**, 090001 (2014).

[11] C. Bobeth *et al.*, *Phys. Rev. Lett.* **112**, 101801 (2014).

[12] V. Khachatryan *et al.* [CMS Collaboration], R. Aaij *et al.* [LHCb Collaboration], *Nature* **525**, 68 (2015).

[13] R. Aaij *et al.* [LHCb Collaboration], Angular Analysis of the $B^0 \to K^{*0}\mu^+\mu^-$, LHCb-CONF-2014-002, 2015.

[14] S. Descotes-Genon, L. Hofer, J. Matias, J. Virto, *J. High Energy Phys.* **1412**, 125 (2014).

[15] A. Bharucha, D. Straub, R. Zwicky, `arXiv:1503.05534 [hep-ph]`.

[16] C. Bobeth, G. Hiller, D. van Dyk, C. Wacker, *J. High Energy Phys.* **1201**, 107 (2012).

[17] R. Aaij *et al.* [LHCb Collaboration], *J. High Energy Phys.* **1406**, 133 (2014).

[18] R. Aaij *et al.* [LHCb Collaboration], *J. High Energy Phys.* **1509**, 179 (2015).

[19] R. Aaij *et al.* [LHCb Collaboration], *J. High Energy Phys.* **1506**, 115 (2015).